AFRL-VS-HA-TR-2005-1161

Contributions of the OH Airglow to Resident Space Object Irradiance

John Gruninger
James W. Duff

Spectral Sciences, Inc.
4 Fourth Avenue
Burlington, MA 01803-3304

Interim Scientific Report

25 October 2005

APPROVED FOR PUBLIC RELEASE; DISTRIBUTION UNLIMITED.

AIR FORCE RESEARCH LABORATORY
Space Vehicles Directorate
29 Randolph Road
AIR FORCE MATERIEL COMMAND
Hanscom AFB, MA 01731-3010

This technical report has been reviewed and is approved for publication.

AFRL-VS-HA-TR-2005-1161

/signed/	/signed/
JAMES H. BROWN Contract Manager	ROBERT BELAND, Chief Battlespace Surveillance Innovation Center

This report has been reviewed by the ESC Public Affairs Office (PA) and is releasable to the National Technical Information Service (NTIS).

Qualified requestors may obtain additional copies from the Defense Technical Information Center (DTIC). All others should apply to the National Technical Information Service.

If your address has changed, if you wish to be removed from the mailing list, or if the addressee is no longer employed by your organization, please notify AFRL/VSIM, 29 Randolph Rd., Hanscom AFB, MA 01731-3010. This will assist us in maintaining a current mailing list.

Do not return copies of this report unless contractual obligations or notices on a specific document require that it be returned.

Using Government drawings, specifications, or other data included in this document for any purpose other than Government procurement does not in any way obligate the U.S. Government. The fact that the Government formulated or supplied the drawings, specifications, or other data does not license the holder or any other person or corporation; or convey any rights or permission to manufacture, use, or sell any patented invention that may relate to them.

This report is published in the interest of scientific and technical information exchange and its publication does not constitute the Government's approval or disapproval of its ideas or findings.

REPORT DOCUMENTATION PAGE

Form Approved
OMB No. 0704-0188

1. REPORT DATE *(DD-MM-YYYY)*	2. REPORT TYPE	3. DATES COVERED *(From - To)*
25-10-2005	Scientific, Interim	March 2005 – September 2005

4. TITLE AND SUBTITLE

Contributions of the OH Airglow to Resident Space Object Irradiance

5a. CONTRACT NUMBER
F19628-02-C-0078

5b. GRANT NUMBER

5c. PROGRAM ELEMENT NUMBER
62601F

John Gruninger and James W. Duff

5d. PROJECT NUMBER
1010

5e. TASK NUMBER
HS

5f. WORK UNIT NUMBER
A1

7. PERFORMING ORGANIZATION NAME(S) AND ADDRESS(ES)

Spectral Sciences, Inc.
4 Fourth Avenue
Burlington, MA 01803-3304

8. PERFORMING ORGANIZATION REPORT NUMBER

SSI-TR-464

9. SPONSORING / MONITORING AGENCY NAME(S) AND ADDRESS(ES)

Air Force Research Laboratory
29 Randolph Road
Hanscom AFB, MA 01731-3010

10. SPONSOR/MONITOR'S ACRONYM(S)
AFRL/VSBYB

11. SPONSOR/MONITOR'S REPORT NUMBER(S)
AFRL-VS-HA-TR-2005-1161

12. DISTRIBUTION / AVAILABILITY STATEMENT

Approved for Public Release; Distribution Unlimited.

13. SUPPLEMENTARY NOTES

14. ABSTRACT

A goal of space situational awareness is the detection and characterization of resident space objects. An around-the-clock capability depends on the ability to observe the space object under a variety of illumination conditions. In this report, we focus on space-based sensors operating in the visible, near-infrared and short-wave infrared where reflected light sources are the dominant signature components. Of particular interest is the ability to observe space objects from above during nighttime in a moonless sky. A promising illumination source is the hydroxyl radical airglow. It is the most dominant illumination source under these conditions. A further advantage is the location of the airglow between 80 km and 90 km. By being well above the ground, it illuminates surfaces that are pointing upward and hence are observable from above. We predict surface irradiance of space objects as a function of surface orientation for a number of spectral bands, using SAMM2 to compute LOS radiances. A few sample calculations of sensor irradiance for nadir and limb viewing of a space object (modeled as a flat plate) illustrate the ability to observe a space object from above. The requirements of an around-the-clock modeling capability are briefly outlined.

15. SUBJECT TERMS
Visible, Near-Infrared, OH Airglow, Resident Space Object

16. SECURITY CLASSIFICATION OF:			17. LIMITATION OF ABSTRACT	18. NUMBER OF PAGES	19a. NAME OF RESPONSIBLE PERSON
a. REPORT	b. ABSTRACT	c. THIS PAGE			James H. Brown
UNCLASSIFIED	UNCLASSIFIED	UNCLASSIFIED	SAR	22	19b. TELEPHONE NUMBER *(include area code)* 718-377-4412

CONTENTS

FIGURES

TABLES

1. INTRODUCTION

In this report, we investigate the contributions of the hydroxyl (OH) airglow to the illumination of resident space objects. During nighttime, in a moonless sky, the airglow is the largest contributor to the sky brightness in the visible (vis), the near-infrared (NIR) and short-wave infrared (SWIR) spectral region. The dominant contributors to the airglow are vibrationally excited hydroxyl radicals, OH(υ). The radicals are formed in vibrational states up to υ=9 by the reaction of hydrogen atoms with ozone. The strong emissions, known as Meinel emissions, are sequences with $\Delta\upsilon$= 1-6. Emissions with $\Delta\upsilon$= 3, 4, 5 and 6 occur in the visible and NIR between .4 μm and 1.0 μm. From 1.0 μm to 2.5 μm there are very strong emissions from the $\Delta\upsilon$= 2 sequences. The $\Delta\upsilon$= 1 emissions extend into the thermal infrared to 4.5 μm. In this report, we considered four band passes, a vis-NIR band pass, two SABER band passes centered at 1.6 μm and 2.0 μm, respectively, and a broad band pass around 2.7 μm.

In Section 2, the computation of radiance spectra and in-band radiances are discussed. SAMM2 [Dothe *et al.,* 2004] was utilized to compute spectra, and line of sight radiances for an observer on a space platform, looking above the horizon (ATH) and below the horizon (BTH). In Section 3, the use of the line of sight (LOS) radiances to compute the irradiance on a space object is discussed. The space object is taken as a flat plate with a Lambertian surface reflectance. The irradiance depends on the orientation and altitude of the flat plate or facet. Profiles of irradiance versus orientation were calculated. The OH airglow altitude ranges from 80 to 90 km and will illuminate a facet even if it is pointing somewhat upward. The irradiance of the surface was found to be at half its maximum for surface normal point upward at 120^0 (100^0) off nadir for the surface at 250 km (900 km) in altitude, respectively, for the vis-NIR and SABER band passes. An irradiated surface can be seen from above in either ATH or BTH viewing. The irradiance in the 2.7 μm band pass comes almost entirely from the atmosphere in the low altitude and the earth emission.

In Section 4, a few sample calculations of sensor irradiance for nadir and limb viewing of a space object (modeled as a flat plate) illustrate the ability to observe a space object from above. The requirements of an around-the-clock modeling capability are briefly outlined in Section 5.

2. BACKGROUND RADIANCE

The background radiance was computed for four band passes, a vis-NIR band pass from 0.4 μm to 1.0 μm, two SABER band passes [one centered at 1.6 μm (approximately 1.57 μm – 1.73 μm), the second centered at 2.0 μm (approximately 1.94 μm - 2.2 μm)], and a 2.7 μm band pass (2.6 μm to 3.3 μm). SAMM2 predicted limb spectra at 80 km tangent altitude for the four band passes are illustrated in Figure 1. The OH emissions are strong spikes in all four bands. The spectral resolution in the vis-NIR band pass is 5 cm^{-1}, while the spectral resolution in the remaining band passes is 0.5 cm^{-1}. Band pass radiances for ATH and BTH viewing are reported for the four bands in Figures 2, 3, 4, and 5. The radiances are reported in terms of tangent point altitude so that they correspond to those of a sensor at any altitude in space above the atmosphere. A negative tangent point altitude corresponds to a BTH LOS that terminates at the earth but if the line were extended it would penetrate the earth to a depth of the magnitude of this negative tangent point value. The magnitude of the most negative value corresponds to the radius of the earth, 6378 km, and this LOS is nadir. In addition to the band pass radiances that include the OH airglow, radiances in the absence of the OH airglow were also computed to determine the importance of the airglow contribution.

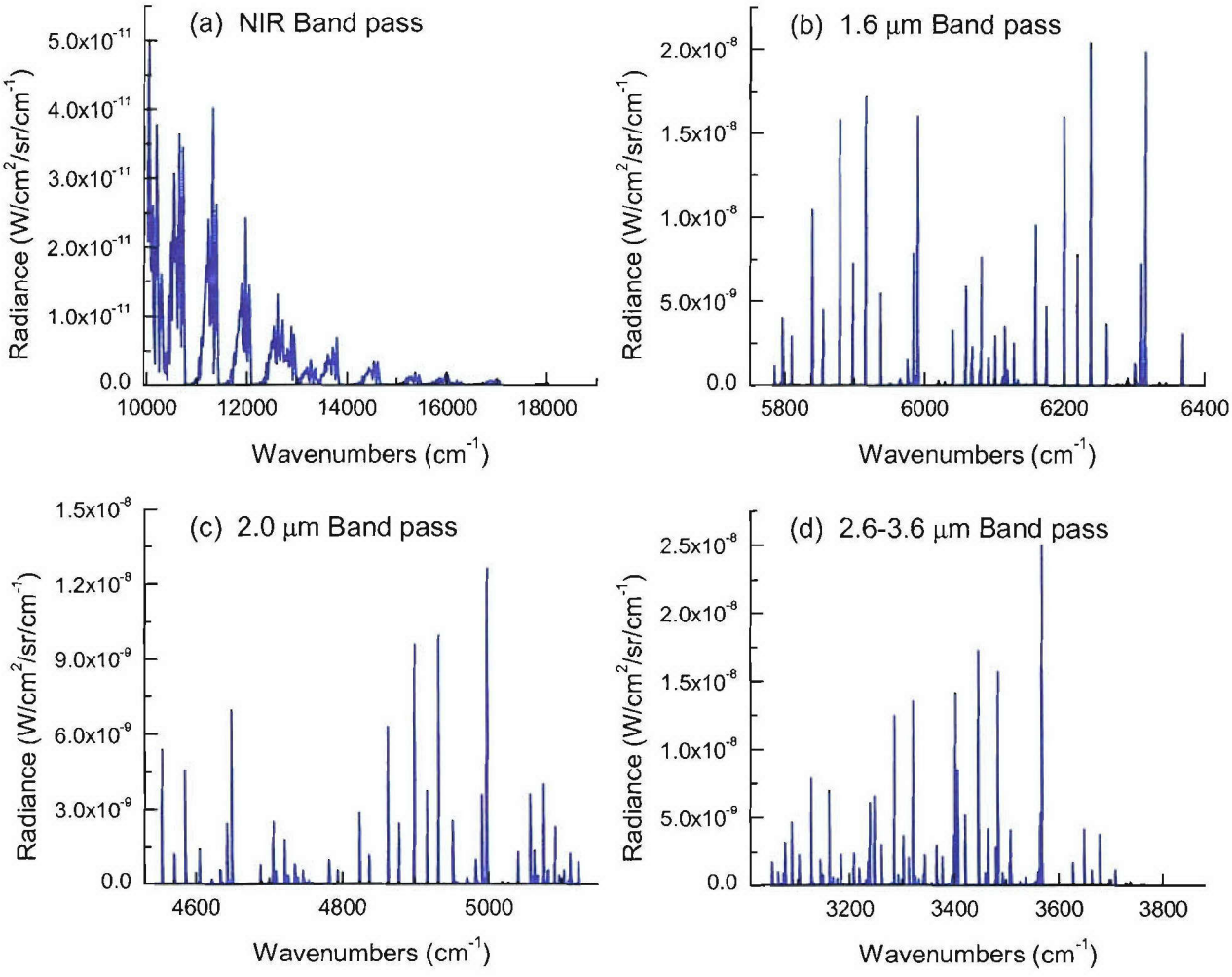

Figure 1. Spectral radiance for an 80 km nighttime limb LOS for (a) A vis-NIR band pass at a spectral resolution of 5.0 cm^{-1}, (b) The SABER 1.6 μm band pass at a spectral resolution of 0.5 cm^{-1} ,(c) The SABER 2.0 μm band pass at a spectral resolution of 0.5 cm^{-1} and (d) The 2.6-3.3 μm band pass at a spectral resolution of 0.5 cm^{-1}.

In Figures 2a and 2b, the background radiances in the 0.4 to 1.0 μm band pass that include the OH airglow are illustrated for ATH and BTH viewing, respectively. The maximum in the radiance occurs for the LOS which has the longest path through the airglow region at a tangent height of 82-83 km. The minimum occurs at nadir viewing which corresponds to the shortest path through the airglow region. The maximum is approximately 60 times as large as the minimum. Figures 2c and 2d illustrate the background radiances in the 0.4 to 1.0 μm band pass in the absence of the OH airglow for ATH and BTH viewing, respectively. In the absence of the airglow, the atmosphere is almost black with radiances that are greater than ten orders of magnitude below those of the OH airglow. The maximum occurs for a 0 km limb view corresponding to contributions in the lower atmosphere below 10 km.

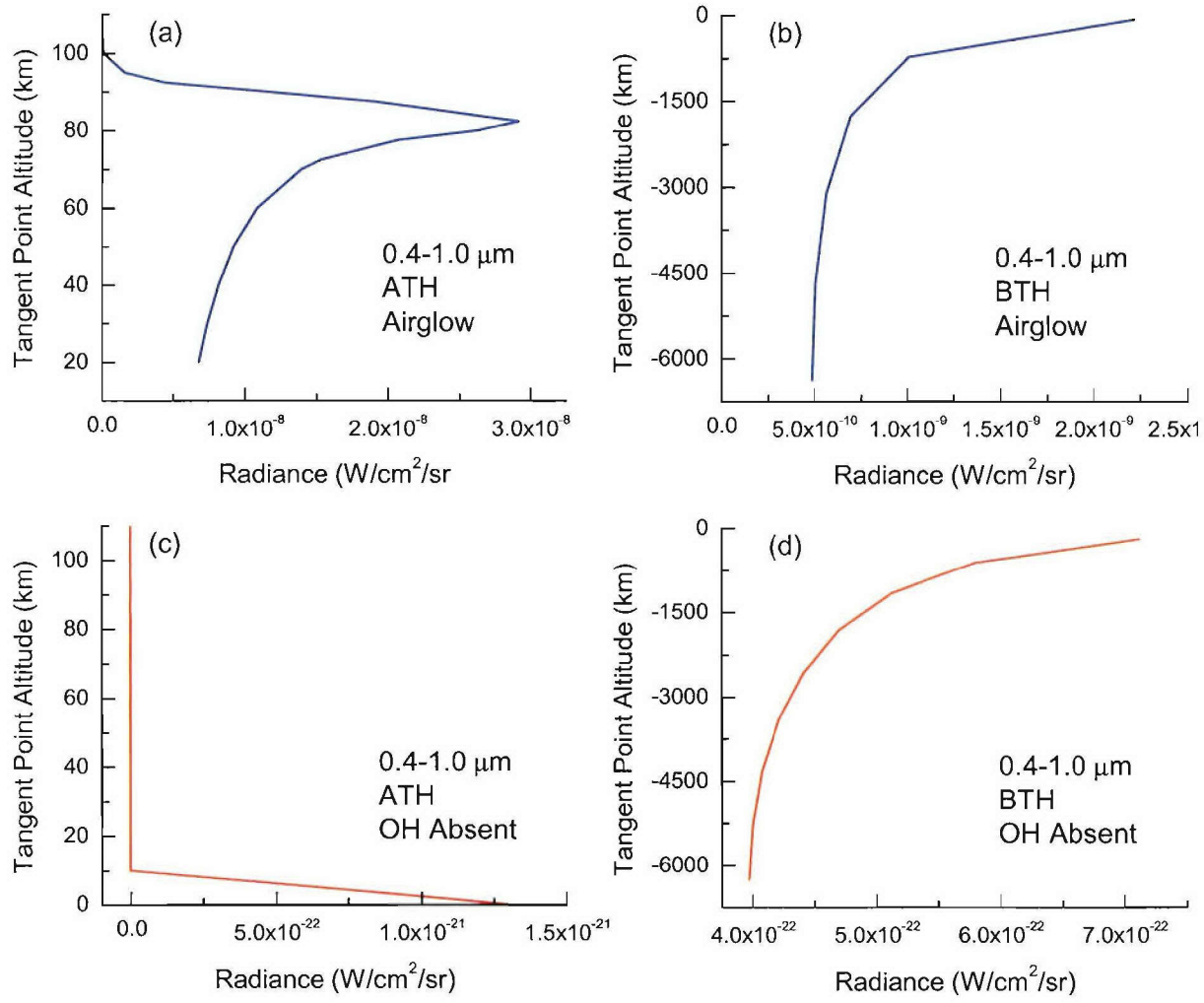

Figure 2. In-band radiance for the 0.4-1.0 μm vis-NIR band pass as a function of tangent point altitude for (a) ATH viewing of the background and airglow, (b) BTH viewing of the background and the airglow, (c) ATH viewing of the background in the absence of the airglow, (d) BTH viewing of the background in the absence of the airglow.

Figures 3a and 3b show the calculated ATH and BTH background radiances in the SABER 1.6 μm band pass that include the OH airglow, respectively. As in the vis-NIR band, the maximum radiance in this SWIR band occurs for the LOS with the longest path through the airglow region, with the smallest at nadir. The ratio of maximum to minimum radiance is about 57/1. Figures 3c and 3d illustrate the background radiances in the SABER 1.6 μm band pass in the absence of the OH airglow for ATH and BTH viewing, respectively. Again the maximum occurs for a 0 km limb view. The airglow radiances are more that four orders of magnitude greater that the other contributions to radiance.

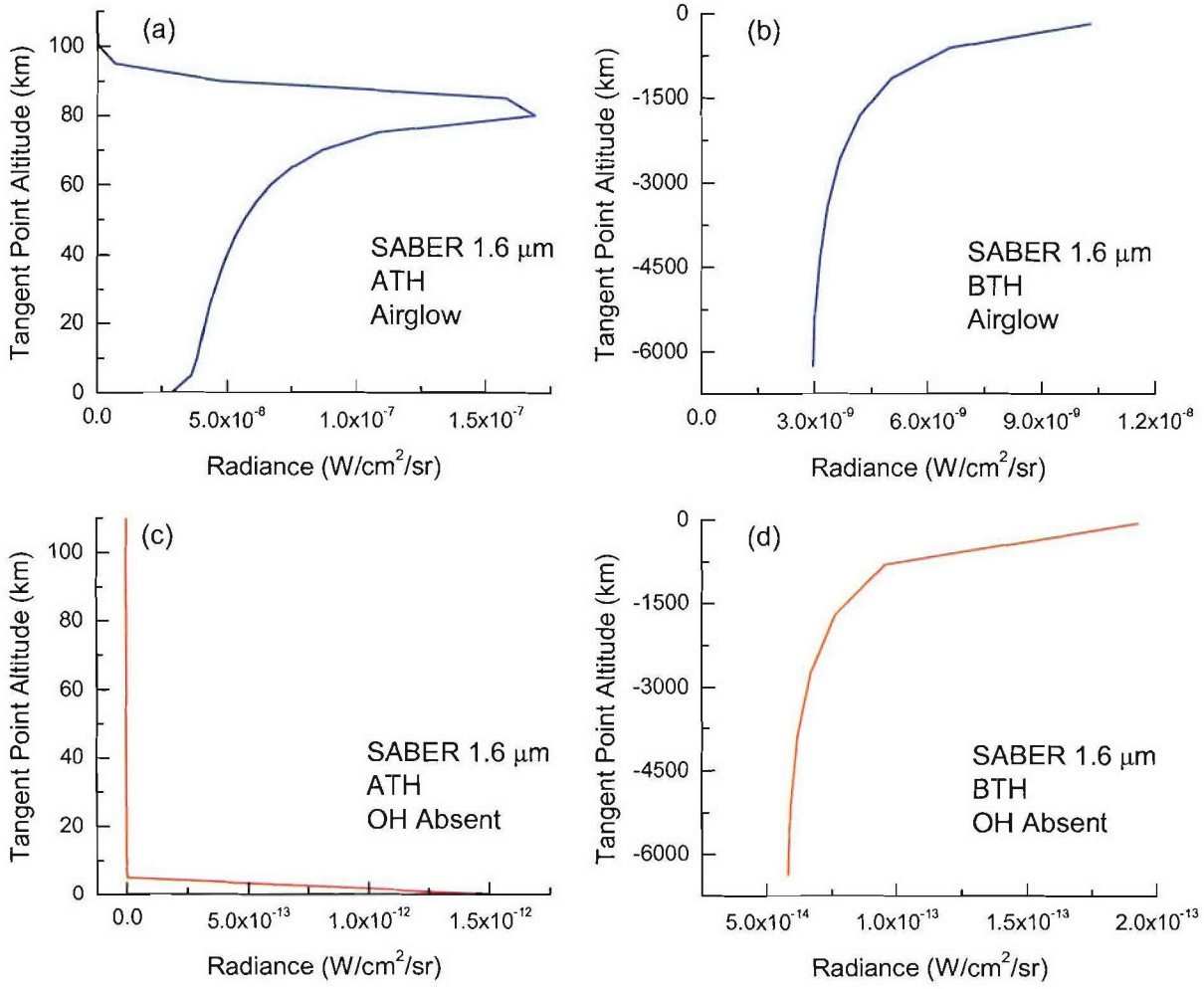

Figure 3. In-band radiance for the SABER 1.6 μm band pass as a function of tangent point altitude for (a) ATH viewing of the background and airglow, (b) BTH viewing of the background and the airglow, (c) ATH viewing of the background in the absence of the airglow, (d) BTH viewing of the background in the absence of the airglow.

In Figures 4a and 4b, the background radiances in the SABER 2.0 μm band pass that include the OH airglow are illustrated for ATH and BTH viewing, respectively. As in the other bands, the maximum radiance occurs for the LOS with the longest path through the airglow region with the smallest at nadir. The ratio of maximum to minimum radiance is about 55/1. Figures 4c and 4d illustrate the background radiances in the SABER 2.0 μm band pass in the absence of the OH airglow for ATH and BTH viewing, respectively. The maximum radiance occurs for a 0 km limb view. The contributions from the lower atmosphere are increased in this band pass with lower altitude BTH radiance contributing a few percent of the total.

In Figures 5a and 5b, the background radiances in the 2.7 μm band pass are illustrated for ATH and BTH viewing, respectively. While there is a large spike in LOS radiance in the limb paths through the airglow, the low altitude limb radiances are larger and the BTH path radiances are larger by a factor of three to four. In this band pass the earth surface emissions and low altitude atmospheric emissions dominate. The contribution of the airglow to the radiances in the low altitude limb and BTH is a few percent.

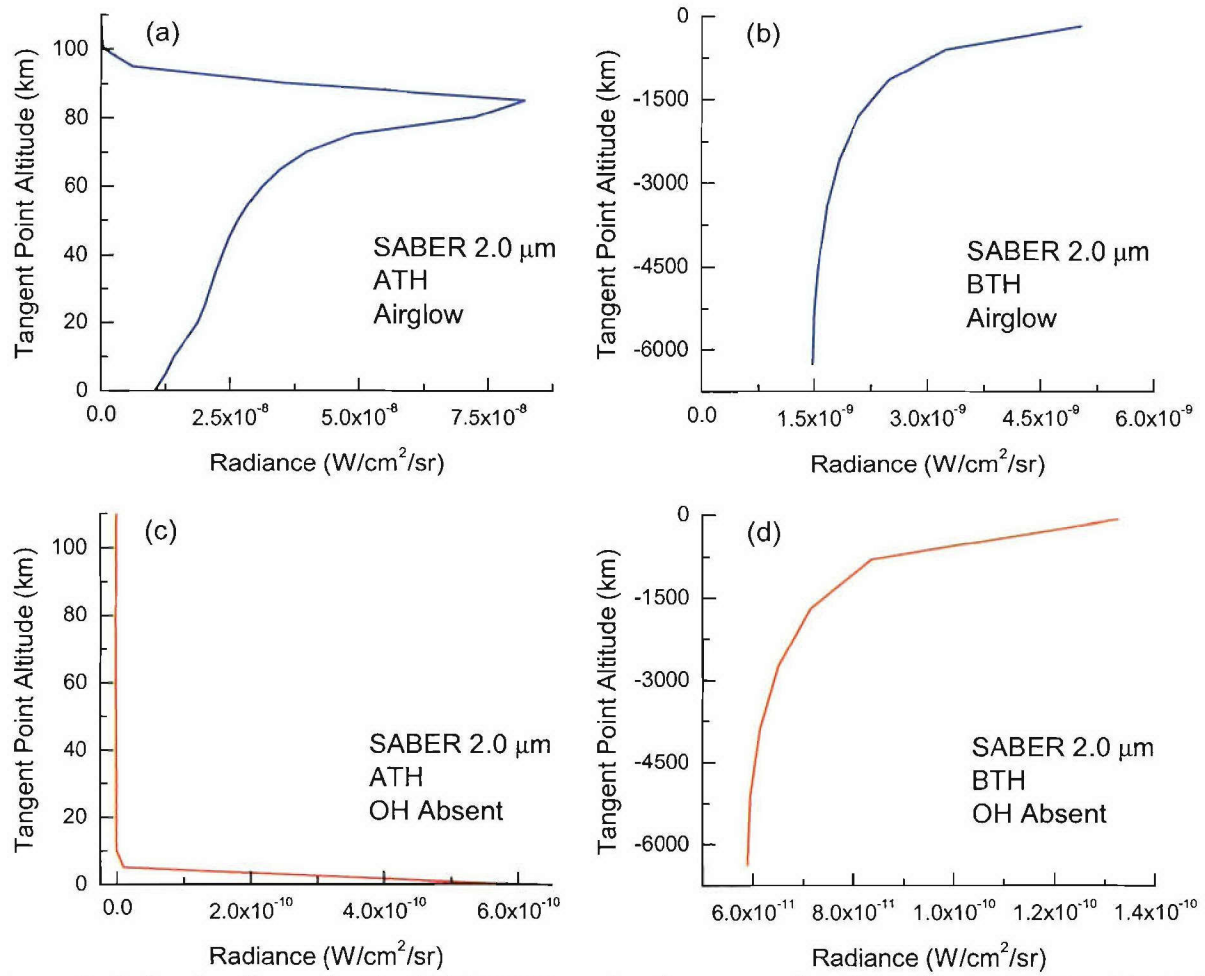

Figure 4. In-band radiance for the SABER 2.0 μm band pass as a function of tangent point altitude for (a) ATH viewing of the background and airglow, (b) BTH viewing of the background and the airglow, (c) ATH viewing of the background in the absence of the airglow, (d) BTH viewing of the background in the absence of the airglow.

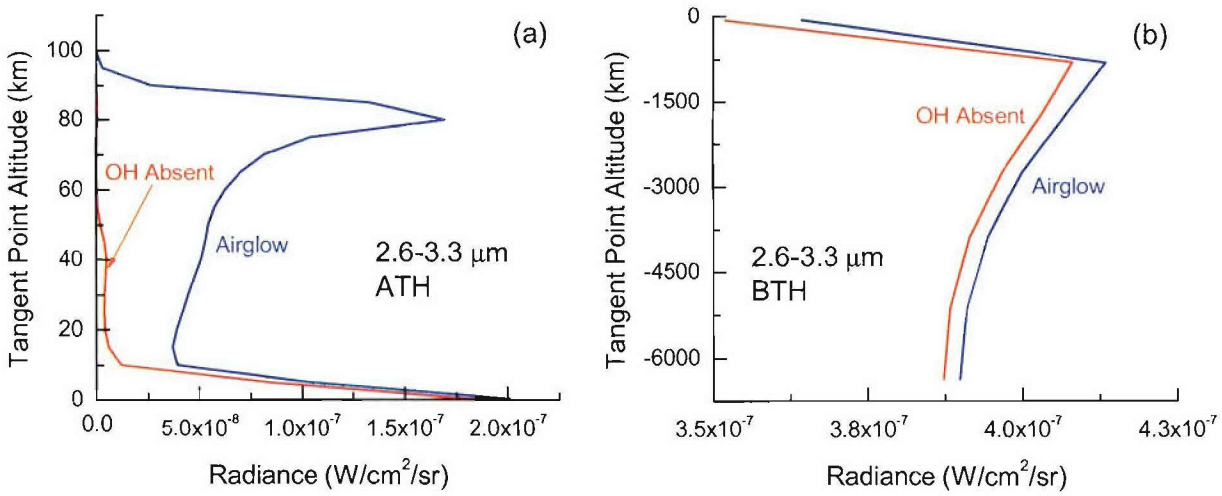

Figure 5. In-band radiance for the 2.6-3.3 μm band pass as a function of tangent point altitude for (a) ATH viewing of the background including and not including the OH airglow, (b) BTH viewing of the background including and not including and the OH airglow.

3. SPACE OBJECT ILLUMINATION AND IRRADIANCE

The irradiance of the surface of a space object depends on its orientation and what is in its viewing hemisphere. For a geometrically complex object, a surface may have a portion of sky and earth obscured by other parts of the object. In this effort, the goal is to assess the importance of the OH airglow in the illumination of space objects. For this purpose it is adequate to consider a flat plate (facet) and to determine its irradiance as a function of its surface normal in the band passes considered. It is further assumed that the facet has a Lambertian surface and a wavelength independent reflectance/emissivity.

The facet irradiance is computed from a hemispherical integration. Allowing the polar angle, Θ, to be measured from the facet normal, the contribution from the light source(s) in the solid angle, $d\omega = \sin\Theta d\Theta d\Phi$, is $L(\Theta,\Phi)d\omega$, where $L(\Theta,\Phi)$ is the radiance arriving at the surface from the Θ,Φ direction. The irradiance is given by

$$H_f = \int_{-\pi}^{\pi}\int_{0}^{2\pi} L(\Theta,\Phi)\cos(\Theta)\sin(\Theta)d\Theta d\Phi$$

In the absence of the solar terminator or aurora, the atmosphere can be assumed to be horizontally isotropic, and the irradiance is only a function of the component of the surface normal relative to the vertical. In the case of horizontal symmetry about the vertical in the atmosphere, the radiance only depends on the angle between the vector in the Θ,Φ direction and the atmospheric vertical. The radiances computed and illustrated in Figures 2-5 are used to compute facet irradiance. The facet irradiance was computed for a grid of facet orientations with facet normal off-nadir angles varying from 0^0 (nadir) to 180^0 (zenith).

In addition to orientation, the irradiance depends on the altitude of the space object, particularly for band passes where the airglow is important. The OH airglow region occurs between 80 km and 90 km. For space objects at low altitude the airglow is well off nadir, while for space objects at high altitude the airglow is closer to nadir. In this effort, we considered two altitudes, one close to typical space shuttle altitude of 250 km and a second altitude of 900 km. In Figures, 6-9, the irradiances of a flat plate at 250 km and 900 km as a function of the off-nadir angle of the surface normal are illustrated. The irradiances in the 0.4 μm-1.0 μm and the SABER band passes are qualitatively similar. Most of the illumination is coming from the airglow, and the maximum in irradiance is off nadir. The atmospheric radiance from the lower altitude increases with wavelength being several orders of magnitude smaller in the 0.4 μm -1.0 μm, while the low altitude radiance contributes a few percent in the SABER 2.0 μm band pass. In the 2.7 μm band pass, illustrated in Figure 9, the maximum irradiance occurs when the surface normal is nadir. The contributions from the lower altitude and ground emissions far exceed the contribution of the airglow to the irradiance. Table 1 shows values of irradiance for a surface normal orientation of 110^0 off-nadir for the three band passes that have a substantial airglow component. For this angle, the surface is pointing slightly upward and reflections from the surface will illuminate sensors that are above it.

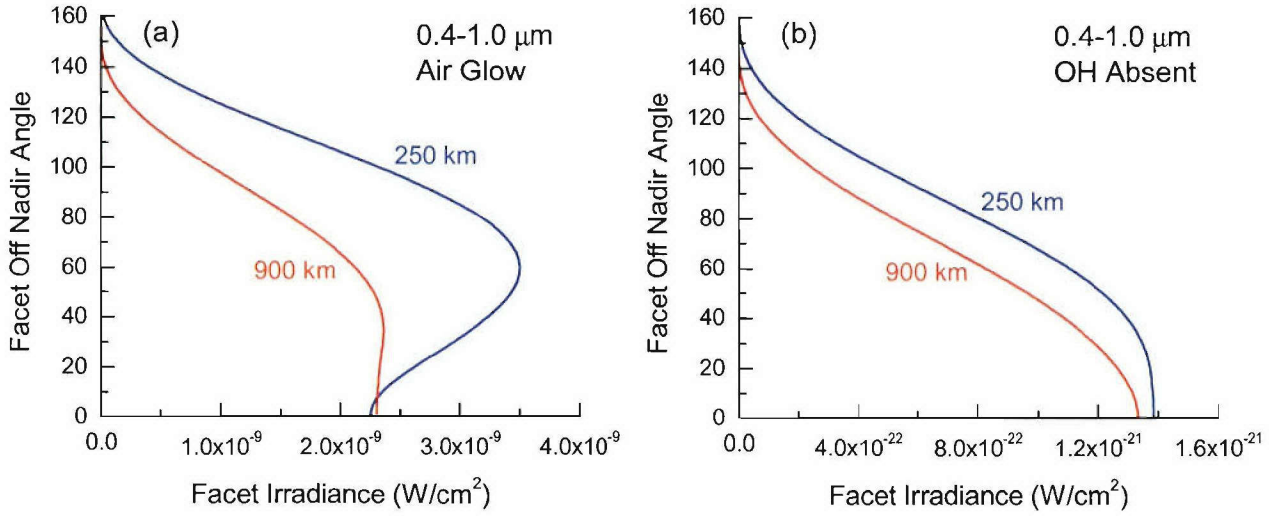

Figure 6. Surface irradiance in the 0.4-1.0 μm band pass of a flat plate at altitudes of 250 km and 900 km as a function of surface orientation for (a) background including OH airglow, (b) background in the absence of the OH airglow.

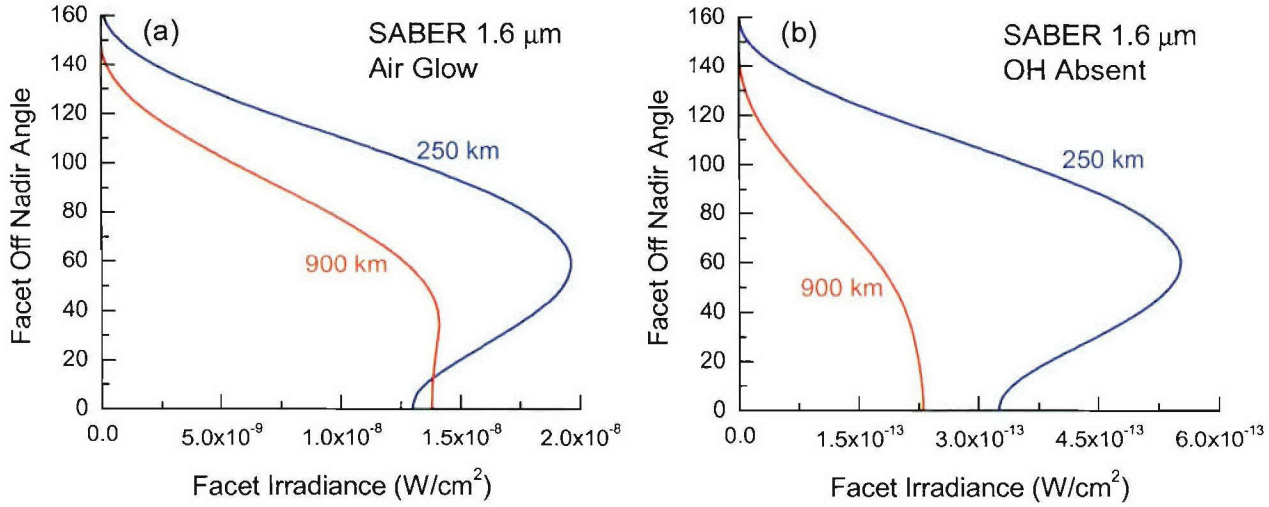

Figure 7. Surface irradiance in the SABER 1.6 μm band pass of a flat plate at altitudes of 250 km and 900 km as a function of surface orientation for (a) background including OH airglow, (b) background in the absence of the OH airglow.

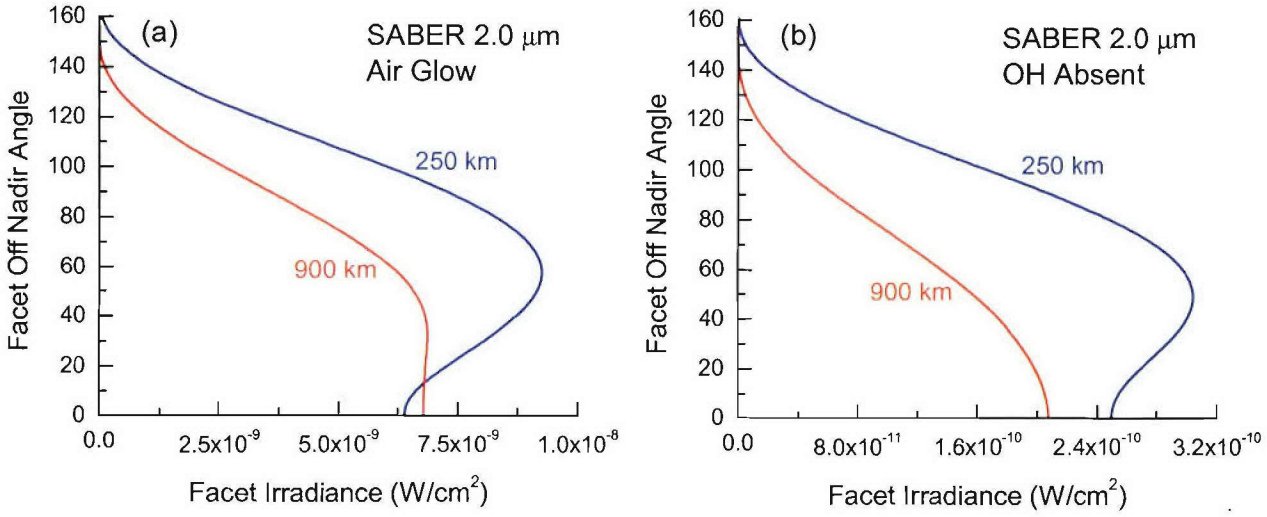

Figure 8. Surface irradiance in the SABER 2.0 μm band pass of a flat plate at altitudes of 250 km and 900 km as a function of surface orientation for (a) background including OH airglow, (b) background in the absence of the OH airglow.

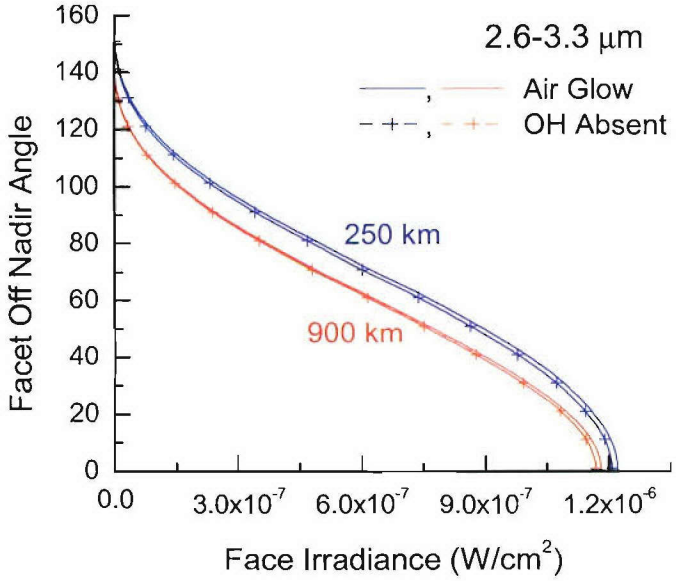

Figure 9. Surface irradiance in the 2.6-3.3 μm band pass of a flat plate at altitudes of 250 km and 900 km as a function of surface orientation for background including OH airglow and in the absence of the OH airglow.

Table 1. Irradiance values for a facet at 110^0 off nadir in W/cm^2

	0.4-1.0 μm	**1.6 μm**	**2.0 μm**
250 km (airglow)	1.8×10^{-9}	1.0×10^{-8}	4.6×10^{-9}
250 km (no airglow)	3.2×10^{-22}	2.7×10^{-13}	1.2×10^{-10}
900 km (airglow)	6.1×10^{-10}	3.6×10^{-9}	1.7×10^{-9}
900 km (no airglow)	1.5×10^{-22}	4.1×10^{-14}	2.6×10^{-11}

4. SENSOR IRRADIANCE FROM REFLECTED AIRGLOW

The light reaching a sensor that is reflected from an illuminated space object depends on the viewing geometry and range from the sensor to the object. We consider a simple case here of a flat plate with a reflectance, ρ, independent of wavelength, a greybody. For a greybody, the sensor irradiance, H_s, can be obtained directly from the band pass integrated facet irradiance H_f. Given H_f, the projected area of the facet , A_p , toward the sensor and the range of the facet from the sensor, R, the sensor irradiance is given by

$$H_s = \rho H_f A_p \tau / R^2$$

where τ is the atmospheric path transmittance between the space object and the sensor. For the sensor above the space object, the atmospheric path is optically thin and τ is essentially unity. For a greybody, we can use the band pass facet irradiances in Figures 6-9 to estimate sensor irradiance due to the reflected background. To illustrate the calculation of sensor irradiance, a flat plate with its surface normal pointing at 110^0 off-nadir is selected. Values of facet irradiance for this orientation appear in Table 1 for the bands that have substantial contributions from the airglow. A surface area of 10 m^2 and a greybody reflectance of 0.7 are assumed. We consider the effect of altitude of the flat plate as well as sensor geometry defined by:

- If the flat plate is at 250 km altitude and the sensor is at 900 km altitude looking nadir, the projected area toward the sensor is 10 m^2 $\cos(180^\circ - 110^\circ) = 3.4$ m^2 and the range is 650 km. The sensor irradiance is equal to $5.6 \times 10^{-12} H_f$. For the same flat plate observed at the tangent point for the sensor looking limb, the projected area is 10 m^2 $\cos(110^0 - 90^0) = 9.4$ m^2 and the range from the sensor is 1849 km. The resulting sensor irradiance is $1.9 \times 10^{-12} H_f$.
- If the flat plate is at 900km altitude and the sensor at 1000 km altitude looking nadir at a range of 100 km or limb with the plate at the tangent point range of 1211 km, the sensor irradiances due to the reflected skyshine are $2.9 \times 10^{-10} H_f$ and $2.7 \times 10^{-12} H_f$, respectively.

The results are also summarized in Table 2.

Table 2. Sensor Irradiance from Reflected Airglow

Altitude of Flat Plate (km)	Sensor Altitude (km)	Sensor Viewing Geometry	Sensor Irradiance (W/cm^2)
250	900	nadir	$5.6 \times 10^{-12} H_f$
		limb	$1.9 \times 10^{-12} H_f$
900	1000	nadir	$2.9 \times 10^{-10} H_f$
		limb	$2.7 \times 10^{-12} H_f$

Observing space objects in BTH viewing has the advantage of shorter ranges, however this is offset by the magnitude of the background radiance. In BTH viewing, the background includes the airglow. For limb viewing with tangent altitudes above the airglow, the background radiance is negligible.

The nighttime natural background irradiances of space objects in the 0.4 -1.0 μm band pass and the SABER 1.6 μm comes essentially totally from the airglow. If the airglow is well-characterized, then the light source is well-characterized in these bands and it may be possible to extract spectral features of the illuminated space objects. For a material reflectance that depends on wavelength, the spectral skyshine and earthshine radiance $L(\Theta, \Phi, \lambda)$, must be used to compute a spectral facet irradiance, $H_f(\lambda)$.

$$H_f(\lambda) = \int_{-\pi}^{\pi} \int_{0}^{2\pi} L(\Theta, \Phi, \lambda) \cos(\Theta) \sin(\Theta) d\Theta d\Phi$$

then the sensor irradiance is given by integration of the spectral sensor irradiance over the band pass.

$$H_s = \int d\lambda H_s(\lambda) = (A_p / R^2) \int d\lambda \rho(\lambda) H_f(\lambda) \tau(\lambda).$$

If both the spectral irradiance and the atmospheric illumination are known, then by inversion the spectral reflectance of the space object can be inferred.

5. MODELING SPACE OBJECT SIGNATURES

An around-the-clock 24/7 modeling capability requires a geometric and material description of the space objects and a complete characterization of the light sources. We focus here on the requirements in the vis-NIR-SWIR where reflective properties dominate thermal characteristics of space objects.

5.1. Natural Illumination Sources

During the day, the sun is the major light source. The airglow is still present but its contribution is small compared to direct and scattered sunlight. At dawn or dusk, twilight is an important light source. Twilight is sunlight that is scattered around the edge of the earth. Twilight is important near the poles where it lasts all night in midsummer. In addition to the scattered light, the atmospheric composition of hydroxyl radical and ozone are altered by the increase/decrease in solar pumping thus affecting the airglow. At night, moonlight is the major light source. Moonlight is primarily reflected sunlight. In the absence of the moon, the airglows are the major source in the vis-NIR-SWIR, with the hydroxyl airglow being the most important. In addition, auroras in polar winters are very bright and, as an extended light source, an aurora will irradiate space objects. In addition to these illumination sources space objects can be illuminated from above by planets and stars, as well as Zodiacal light. Planets reflect sunlight and the illumination from planets is comparable to starlight, but both are small nighttime contributors compared to the airglow. Zodiacal light originates from interplanetary dust particles which scatter sunlight and emit thermally. Zodiacal light is an important nighttime source in the long wave infrared atmospheric window and at higher wavelengths. A survey of the nighttime diffuse illumination sources are included in Leinert *et al.* [1998].

5.2. Man-Made Illumination Sources

Lighting sources around population centers are scattered in the troposphere and extend over large areas. Sources include mercury vapor lamps (0.545 μm and 0.575 μm), high pressure sodium lamps (from 0.540 μm to 0.630 μm) and low pressure sodium lamps (0.589 μm). This artificial skyshine has been measured by sensors on the DMSP (Defense Meteorological Satellite Program) satellite. The DSMP is in a sun-synchronous polar orbit with day/night global coverage with a 3 km footprint and a 0.4 μm to 1.1 μm band and an 8 μm to 13 μm thermal band. Measurements in the 0.4 to 1.1 μm band have been extensively studied by Cinzano *et al.*, [2001] and the data have been converted to zenith radiance and an atlas of night sky. The DMSP data and the atlas would be useful input for constructing a model of the contributions of man-made sources to space object illumination. The amount of artificial illumination in remote rural areas is still much smaller than the natural value. Over large urban areas, however, the man-made sources are much larger and artificial illumination is increasing.

5.3. Space Object Models

To simulate the observed radiance from space objects, a geometric model of the surface is required. Typically a facet representation of the space object must be created. This can be accomplished from design drawings or CAD representations. An example facet model for the TAOS satellite is illustrated in Figure 10. Several such models exist. To characterize a space object, its material spectral reflectances are also important. The TAOS satellite consists of an anodized aluminum cylinder and semiconductor solar panels. Figure 11a shows the spectral reflectance of these materials over the range of 0.3 to 15 μm

[Dummer *et al.*, 1993]. The two materials have very different reflective properties. In particular, the solar cell material reflects poorly in the vis-NIR but quite well in the 1.0–2.0 μm spectral band pass, while the anodized Al reflects quite well in all band passes. The range of angles over which a material will have significant reflection is determined by the material's bidirectional reflectance distribution function (BRDF), as shown in Figure 11b [Dummer *et al.*, 1993]. The semiconductor has a sharply peaked BRDF which indicates that reflections off the front of the solar panel will be very sensitive to the illumination-satellite-observer geometry. Consequently, the reflections from this material will occur only over a very small range of angles. The anodized Al has a very broad BRDF and will reflect over a wide range of angles.

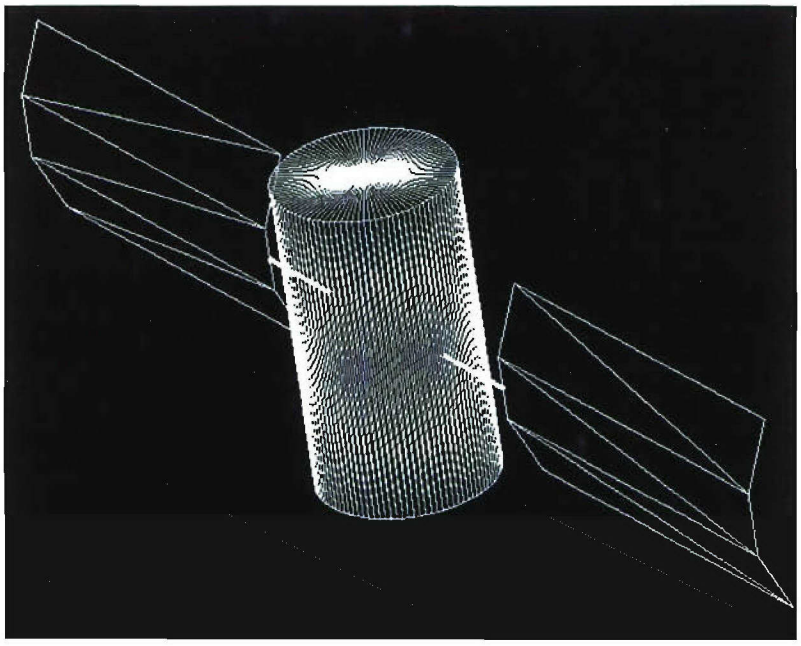

Figure 10. Wireframe image of TAOS satellite model.

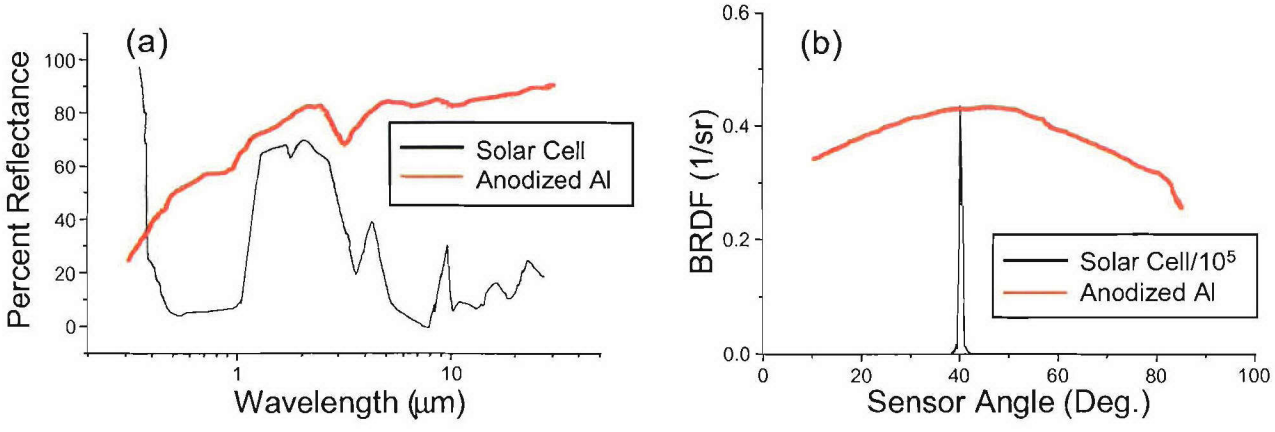

Figure 11. Reflectance properties of TAOS satellite materials: (a) Spectral reflectance and (b) BRDF.

The target signature models, SPIRITS (SPectral and In-band Radiometric Imaging of Targets and Scenes) [Conant *et al.*, 1999] and QUID (Quick Image Display) [Sundberg *et al.*, 1997; 1998] use facet

geometry models. SPIRITS uses software to deal with self-obscuration, while QUID utilizing OPENGL [1993], has the capability of using either software or graphics boards for the self-obscuration problem. The QUID prediction of a solar illuminated radiance image of the TAOS satellite is shown in Figure 12.

Neither SPIRITS or QUID, however, have reflected skyshine models that include important phenomena such as the airglow or terminator effects. Currently, their atmospheric models are based on MODTRAN4 [Anderson *et al.*, 2000] and therefore do not include the important NLTE contributions of the upper atmosphere. In addition, both assume that the sky and earth radiance is isotropic. An accurate treatment will require inclusion of the full angular details of the background radiance, $L(\Theta, \Phi, \lambda)$, and also include the self-obscuration. The radiance that illuminates a facet at a particular orientation may be the background radiance in that direction or it may by a reflection from another portion of the space object that is blocking the line of sight from the facet to the background. A complete model that includes these effects needs to be developed.

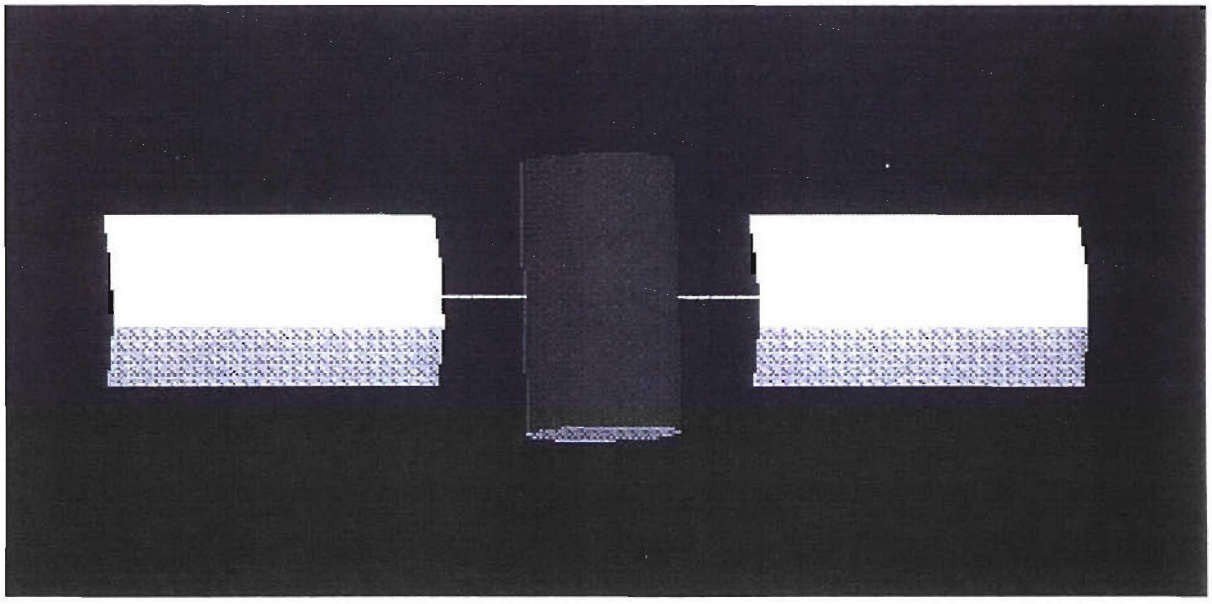

Figure 12. QUID image of TAOS satellite model. The cylinder is modeled as anodized aluminum and the solar panels are modeled using measured reflective properties.

6. CONCLUSIONS

In this report we focused on space-based sensors operating in the visible, near-infrared and short-wave infrared where reflected light sources are the dominant signature components. Of particular interest is the ability to observe space objects from above during nighttime in a moonless sky. The OH airglow altitude ranges from 80 to 90 km and will illuminate surfaces of a space object even if the surfaces are pointing somewhat upward. For the vis-NIR and SABER band passes, the irradiance of the surface was found to be at half its maximum for a surface normal pointing upward at 120^0 off nadir for the surface at 250 km in altitude. For a space object at 900 km in altitude, the half maximum occurs at 100^0 off nadir. An irradiated surface can be seen from above in either ATH or BTH viewing in these band passes. The night-time natural background irradiances of space objects in the 0.4 -1.0 μm band pass and the SABER 1.6 μm band pass comes essentially totally from the airglow. If the airglow is well-characterized spectrally, multispectral sensors with bands in the 0.4 μm – 2.0 μm spectral region will be able to extract spectral features of the illuminated space objects. The irradiance in the 2.7 μm band pass comes almost entirely from the troposphere and earth emission. Curves of object surface irradiance versus surface orientation illustrate the orientation effects and demonstrate the importance of the OH airglow as a

nighttime illumination source. The curves can be used to estimate sensor irradiance resulting from airglow reflected from space object surfaces.

An around-the-clock capability to detect and/or characterize space objects from space rests on the ability to observe and model the space object under a variety of lighting conditions. The necessary modeling features were outlined. A missing element is a sky background illumination model which includes upper atmospheric sources such as the aurora and solar terminator as well as the OH airglow.

References

Anderson, G. P., A. Berk, P. K. Acharya, M. W. Matthew, L. S. Bernstein, J. H. Chetwynd, H. Dothe, S. M. Adler-Golden, A. J. Ratkowski, G. W. Felde, J. A. Gardner, M. L. Hoke, S. C. Richtsmeier, B. Pukall, J. Mello and L. S. Jeong, "MODTRAN4: Radiative Transfer Modeling for Remote Sensing," [4049-16], Algorithms for Multispectral, Hyperspectral and Ultraspectral Imagery VI, Proceedings of SPIE, **4049**, Orlando, FL (2000).

Cinzano, P, F. Falchi, C. D. Elvidge, "The First World Atlas of the Artificial Night Sky Brightness," Mon. Not. R. Astron. Soc., 328, 689-707, (2001).

Conant, J.A., J. F. DeAngelis, S.Y. Yun, D. Drugan, B. P. Sandford, J. H. Schummers, D. C. Robertson, and M. E. Vaughn Jr. "The JANNAF SPectral and In-band Radiometric Imaging of Targets and Scenes (SPIRITS)," AFRL-VS-TR-1999-1550, AFRL/VSBC, 29 Randolph Rd, Hanscom AFB (1999).

Dothe, H., J. W. Duff, J.H. Gruninger, P.K. Acharya, A. Berk, and J.H. Brown, "Users' Manual for SAMM2, SHARC-4 and MODTRAN-4 MERGED," AFRL-VS-HA-TR-2004-1001 (2004).

Dummer, R. S., W. T. Breckenridge, Jr., D. R. Diaddigo, P. M. McKenna, and M. T. Beecroft, "Prediction of Multispectral Observables for the TAOS Satellite," Report No. SOC-R773-001-0293, Surface Optics Corp., San Diego, CA (1993).

Leinert, Ch., S. Bowyer, L. K. Haikala, M. S. Hanner, M. G. Hauser, A. Ch. Levasseur-Regourd, I. Mann, K. Mattila, W. T. Reach, W. Schlosser, H. J. Straude, G. N. Toller, J. L. Weiland, J. L. Weinberg, and A. N. Witt, "The 1997 Reference of Diffuse Night Sky Brightness," Astron. Astrophys. Suppl. Ser. 127, 1-99, (1998).

OpenGL Architecture Review Board, *OpenGL, Reference Manual*, Addison-Wesley, Reading, MA (1993).

Sundberg, R. L., J. Gruninger, M. Nosek, J. Burks, and E. Fontaine, "QUICK IMAGE DISPLAY (QUID) Model For Rapid Real-Time Target Imagery And Spectral Signatures," Proc. SPIE, **3084**, 272 (1997).

Sundberg, R. L., and J. Gruninger, "Quick Image Display (QUID) Model for SPIRITS," 1998 JANNAF SPIRITS User Group Meeting, NASA Kennedy Space Center, FL (1998).